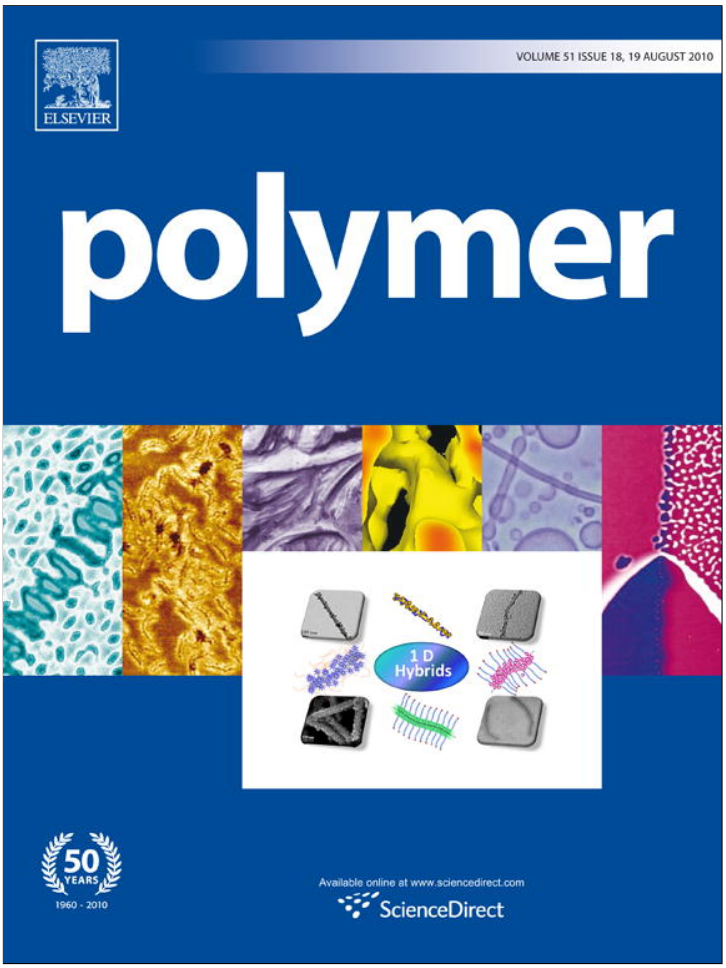

Polymer 51 (2010) 4185–4194

Contents lists available at ScienceDirect

Polymer

journal homepage: www.elsevier.com/locate/polymer

Origin of the melt memory effect in polymer crystallization

José A. Martins [a,b,*], Weidong Zhang [a,b], António M. Brito [a]

[a] Departamento de Engenharia de Polímeros, Universidade do Minho, Campus de Azurém, 4800-058 Guimarães, Portugal
[b] CICECO, Universidade de Aveiro, 3810-193 Aveiro, Portugal

ARTICLE INFO

Article history:
Received 24 May 2010
Received in revised form
5 July 2010
Accepted 6 July 2010
Available online 14 July 2010

Keywords:
Melt memory
Entanglements
Precursor structures

ABSTRACT

Reproducibility of repeated crystallization experiments from melts is obtained after annealing the melt at a sufficiently high temperature for short time, or at lower temperatures for longer time. This annealing process erases the polymer melt memory. Its physical origin remains elusive, but it is linked to precursor structures for crystallization. What precursor structures are, and how they are affected by shear flow and melt temperature is also unclear. We identify in this work two well-defined melt states: the fully relaxed melt and the melt sheared up to a steady state. Crystallization from fully relaxed melts is slowest while from melts sheared up to the steady state is fastest. We demonstrate that polymers crystallized at the same temperature from the two different melt states have similar average spherulite size, but melts sheared up to steady state have lower viscosity and low number of entanglements, this being the reason for the acceleration of crystallization kinetics in these melts. Annealing of the melts sheared up to the steady state slows down the crystallization kinetics until it becomes comparable with that of fully relaxed melts.

1. Introduction

Repeated quiescent crystallization experiments from melts at different temperatures vary with the melt temperature and annealing time. When the melt is heated at a high temperature for a short time or at lower temperatures (always above the melting temperature) for longer time, the memory of previous thermal and mechanical treatments is erased, and crystallization experiments become reproducible [1,2].

At least, two different explanations were given for the erasing of melt memory effect, or more precisely, *the slowing down of crystallization kinetics*. Because according to the classical nucleation theory, active nuclei are generated from embryos existing in the supercooled melt, it was considered that at high temperatures, even when the annealing treatment is performed for longer time, some embryos must survive, becoming latter active nuclei [1]. The slowing down of crystallization was explained as resulting from the embryos' destruction by the annealing treatment. No physical argument was presented to explain why some privileged embryos should survive at high temperatures, even above the equilibrium melting temperature, for a longer time (see Fig. 5 in Ref. [1]). The other explanation considers precursor structures for crystallization, which are also embryos, but are considered in different perspectives by different authors.

Some authors consider that nucleation precursors are only created by shear flow, being absent in quiescent melts with their melt memory erased [3,4]. It is considered that flow causes the orientation of polymer molecules, promoting the alignment and chain interactions, increasing the number of stable nuclei and accelerating the crystallization kinetics [4]. By making basic considerations about relevant relaxation times and chain dynamics, we will show below that this conclusion is not valid for crystallization from pre-sheared melts. The number of surviving nucleation precursors after shear at different melt temperatures was evaluated, and it was found to decrease by increasing the holding time at the melt temperature, the rate of decrease being higher for higher melt temperatures [3]. This assessment was made by evaluating the critical holding time for the disappearance of transcrystalline morphology in fiber pulling experiments, being implicit a link between transcrystalline morphology and shear-induced precursors. None of these works, or others, clarified the origin of precursor structures. They contributed, however, to show that they do not have crystallographic order, survive more than 2 h after cessation of shear and that they are a layer-like superstructure with an average layer spacing of 400 Å [4].

The other perspective considers precursor structures as conceptual objects containing crystallites [2]. It is assumed that

* Corresponding author at: Departamento de Engenharia de Polímeros, Universidade do Minho, Campus de Azurém, 4800-058 Guimarães, Portugal. Tel.: +351 253510325; fax: +351 253510229.
E-mail address: jamartins@dep.uminho.pt (J.A. Martins).

0032-3861/$ – see front matter © 2010 Elsevier Ltd. All rights reserved.
doi:10.1016/j.polymer.2010.07.010

during crystallization its volume grows with time. At high melt temperatures, where the memory effect was erased, the objects are void from crystallites, while at lower melt temperatures they are being progressively filled with crystallites. According to this view, the melt memory effect originates from changes in the creation rate of crystals within the precursor structures. In the conceptual explanation of this model it was also recognized that no direct signals from these objects in their initial form, *i.e.* prior to their filling with crystallites, was detected. Nevertheless, their existence was postulated from the following arguments: 1) their function as a container which offers a crystal nucleation rate much higher than that of the free melt, and 2) the generation of an orientational texture of the crystallites within one object.

The experimental results presented below suggest different explanations for the effect on precursor structures of shear flow, melt temperature, holding time at the melt temperature and the origin of melt memory effect. Because polymer melts are shear-thinning fluids, their viscosity decreases by application of shear, down to a limiting low value for melts sheared up to the steady state. Since diffusion of polymer chains to the spherulite growth front is facilitated in melts with low viscosity, it is expected an enhancement of crystallization kinetics without significant changes in the nucleation density (nuclei with the critical size depend mainly on the surface energies and supercooling degree). This enhancement is recorded and it is demonstrated that no significant changes in the nucleation density occur when relaxed and pre-sheared melts crystallize at the same temperature. It is shown also that annealing melts sheared up to the steady state slows down the crystallization kinetics. The origin of melt memory effect is discussed from these results.

2. Experimental

Experiments were performed with different materials and those presented here refer to an isotactic polypropylene (iPP)–Moplen HP501 M from Basell, Switzerland –, $M_w = 150.8$ kg/mol, $M_w/M_n = 6.15$, $M_z = 488$ kg/mol, $T_m^0 = 210\,^{\circ}C$ and nominal melting temperature of 165 °C [5]. We justify below the use of a commercial polymer grade for these experiments and the validity of results obtained with this polymer.

The analysis of controlled flow deformations' effects applied above the melting temperature on the crystallization kinetics was performed in the capillary channel of a shear DTA instrument [5,6]. Further details of this instrument are in Ref. [6]. These deformations were applied by a piston to the molten polymer stored in an accumulator that flows, by a conical channel, to a capillary where thermal analysis measurements are performed.

The effects of flow deformation on crystallization kinetics were evaluated in the capillary channel by measuring the difference of temperature between the sample in the capillary and a reference following the same temperature program. The overall strain applied to a volume element of the polymer melt is obtained by adding the strain values at the different sections of the shear DTA, accumulator, conical channel, and capillary. The results presented below refer to evaluations made at the channel's walls. This evaluation requires knowledge of melt residence time in the different sections and the corresponding shear rate. Evaluation details are in the Appendix.

We follow "the melt memory protocol" illustrated in Fig. 1a. At the start of the experiment, all different parts are heated up to a selected temperature, above the polymer melting temperature. Controlled deformations, with different shear rates and shearing times, are applied to the polymer melt stored in the accumulator. After the desired shearing, valves at the entrance and exit of the capillary are closed for stopping the flow and promoting the thermal insulation between the accumulator and capillary. This channel is cooled to the desired crystallization temperature, and the effect of flow deformations on the crystallization kinetics is recorded in the absence of flow by a set of thermocouples along the length of the capillary.

From this description, it is clear that the philosophy of this melt memory protocol, implemented in the shear DTA instrument, is different from that of other apparently similar experimental setups used to study the effect of shear flow on the enhancement of crystallization kinetics, which are mainly based on the "short-term" shearing protocol, Fig. 1b [7,8]. With this protocol, the effect studied is the enhancement of crystallization kinetics by application of shear deformations at the crystallization temperature, and the strain applied to the melt is limited by length of the duct (around 100 s.u.). Despite the relevant information obtained for the effect of shear stress on the development of the skin-core morphology [8] and the explanation provided for the development of shish-kebab structures [9], there are several problems with protocol. Since with this protocol shear deformations are applied to the hotter melt stored in the accumulator that flows to a duct at the crystallization temperature, there is no precise control of the temperature at which crystallization experiments are performed – the hotter melt mixes with the melt at the crystallization temperature. A shortcut to this problem is performing crystallization experiments at high temperatures for allowing time to equilibrate the temperature at the duct. Another problem is the lack of control on the strain applied to the polymer pumped from the accumulator to the duct. Depending on the shear-pulse time duration and intensity, the hotter melt is pumped in short time intervals, which are followed by relatively long time intervals for recording the crystallization, the melt at the accumulator may relax fully, or that relaxation may be incomplete. This lack of control of melt deformation at the accumulator [8], or extruder [7] inhibits the use of "short-term" shearing protocol for studying the origin of melt memory effect.

In the shear DTA much larger deformation values can be applied to the polymer melt (values larger than 1000 s.u.). Since some doubts may be cast on the feasibility of these large values, a demonstration of their evaluation is provided in the Appendix. An additional confirmation of these values by a rheometer working with plate–plate and cone-and-plate configurations was given in refs. [5,10]. For clearness of presentation, some of these results are also presented below.

The effect described in this work is the ability of the melt sheared above its melting temperature storing the memory of flow deformations, and the effect of these deformations on the supercooled melt crystallization kinetics at the quiescent state. By adding the strain applied to the melt in the accumulator, conical valve and capillary, much higher strain values are applied to the polymer melt than with the "short-term shearing" protocol. It may be anticipated that the magnitude of this effect on the overall nucleation density is much lower than that of shear deformations applied at the crystallization temperature [8]. This assessment is also demonstrated below with experimental results.

We must emphasize again that all thermal analysis measurements reported in this work are performed in the absence of flow. Because the same melt and crystallization temperatures were used, and also because polymers retain the memory of their previous thermal and flow history, only the flow effects on crystallization development are detected.

3. Results

3.1. Acceleration and saturation of crystallization kinetics in pre-sheared melts

The effect of polymer melt deformation by flow on the crystallization kinetics was presented already in previous works. Here, we provide additional evaluation of possible error sources not

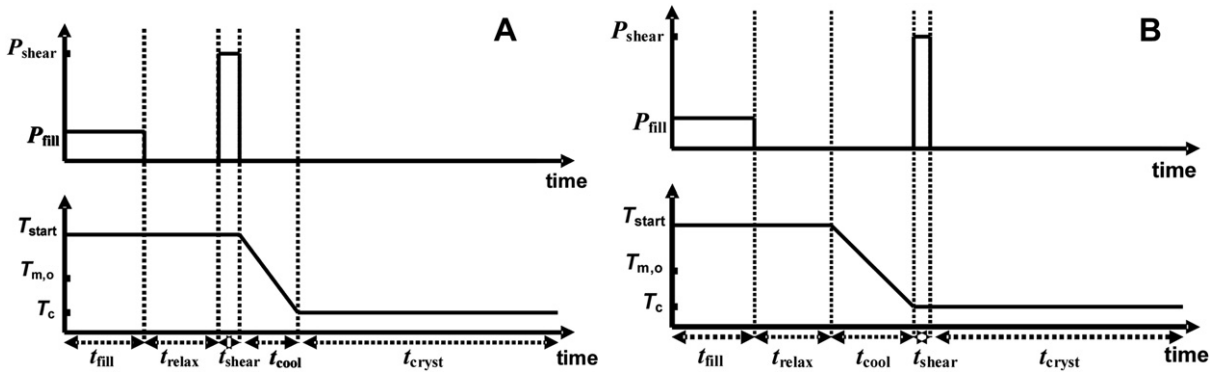

Fig. 1. (**A**) Scheme of the melt memory protocol used in this work for the isothermal experiments. The shear-pulse is applied at the processing temperature and the sheared melt is immediately cooled to the crystallization temperature. Recording of crystallization kinetics is performed in the absence of flow. (**B**) Scheme of the short-term shearing protocol [7,8]. When the polymer is at a nominally isothermal temperature (crystallization temperature), a strong pressure pulse is applied during a short time implying the contact of material at the processing temperature with material at the crystallization temperature. The total strain imposed to the sample was limited to the length of the flow channel. Reprinted with permission from Martins JA et al. Rev Sci Instrum 76, 105105. Copyright 2005, American Institute of Physics.

considered previously and we demonstrate further the origin of melt memory effect.

In previous works [5,10] it was shown that application of shear deformations to polymer melts above the melting temperature, followed by cooling to the crystallization temperature and further recording of crystallization kinetics in the absence of flow, resulted in the acceleration of crystallization and its saturation at a constant strain value. By saturation, we mean that quiescent isothermal [6,10], or non-isothermal [11], crystallization kinetics from melts sheared above the melting temperature cannot be accelerated beyond a limiting low value of half-crystallization time.

Fig. 2 represents a set of results illustrating this behaviour. They were obtained by shearing the melt at 220 °C with constant shearing time of 60 s and increasing shear rates. The isothermal crystallization of a fully relaxed melt is represented by a solid line. Controlled shear deformations applied at the same melt temperature enhance the crystallization kinetics until saturation. The enhancement is indicated by open symbols and saturation is represented by filled symbols. It occurs at a constant strain that depends only on the sheared melt temperature.

Similar experiments were also performed with constant shear rate and increasing shearing time. They show also the acceleration

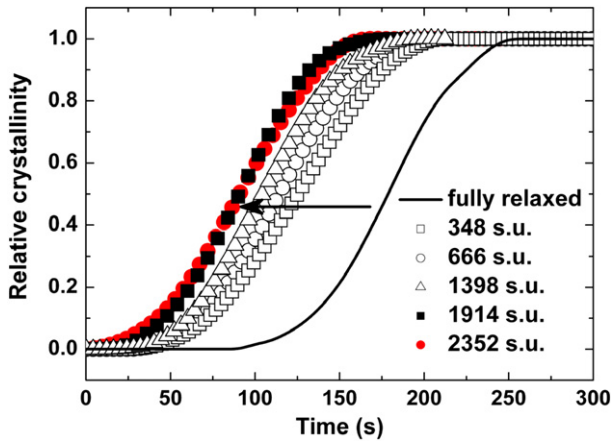

Fig. 2. Acceleration of crystallization kinetics in a fully relaxed melt with application of shear. Melt temperature: 220 °C. Cooling rate to crystallization temperature: −30 °C/min. Crystallization temperature: 125 °C. Before quiescent isothermal crystallization, melts were pre-sheared during 60 s, with shear rates at the channel's wall of 5.8 s^{-1}, 11.1 s^{-1}, 23.3 s^{-1}, 31.9 s^{-1} and 39.2 s^{-1}. The corresponding strain is in the figure legend. Solid line is the crystallization kinetics of a fully relaxed melt. Saturation of crystallization occurs at an average strain of 1970 s.u. (±10%).

of crystallization and its saturation at the same large strain values. In summary, the same final result is obtained regardless if the melt is sheared with increasing shear rates and constant shearing time, or if shearing is applied at a constant shear rate at different shearing time intervals. These results suggest that the strain applied to the melt is the factor controlling the saturation of crystallization from sheared melts. They indicate also that a well-defined melt state should be responsible for this behaviour.

These two conclusions were confirmed further with additional results for: i) the crystallization kinetics of melts at different temperatures while sheared at the same temperature, and ii) the crystallization kinetics of melts at the same temperature while sheared at different temperatures. Both results demonstrate that the strain applied to the melt controls the saturation of crystallization – see results in refs. [5,10]. Most important are the results obtained for melts sheared at different temperatures. It was found that the strain required to saturate crystallization decreases by increasing the melt temperature – filled squares in Fig. 3.

These results raise several questions. The first, and obvious one, is their validity. This is an obligatory question because of the large strain values obtained, because of their temperature dependence, and also because a commercial polymer grade, which has an unknown amount of additives, among them nucleating agents, was used in these experiments. We will answer this question and others below, but first we demonstrate that annealing melts pre-sheared with large strain slows down the crystallization kinetics and that this slowing down is comparable to that recorded for the erasing of melt memory effect.

3.2. Annealing pre-sheared melts with large strain

The strain applied to the melt was evaluated following the procedure described in the Appendix. Because of the observed acceleration in the crystallization kinetics of sheared melts and its saturation at a specific strain value that decreases by increasing the melt temperature, we may conclude that a pure melt effect is responsible for this behaviour. Therefore, annealing of the melt should erase the memory of previous shear deformations, yielding the crystallization kinetics of a relaxed melt.

Fig. 4 demonstrate the progressive erasing of melt memory effect, which results in the slowing down of crystallization kinetics, until after an annealing time of 16 h the crystallization kinetics is again similar to that of a fully relaxed melt. In an attempt to explain these results, we may consider: i) that primary nuclei are destroyed by annealing of the melts and/or ii) that annealing lowers chain

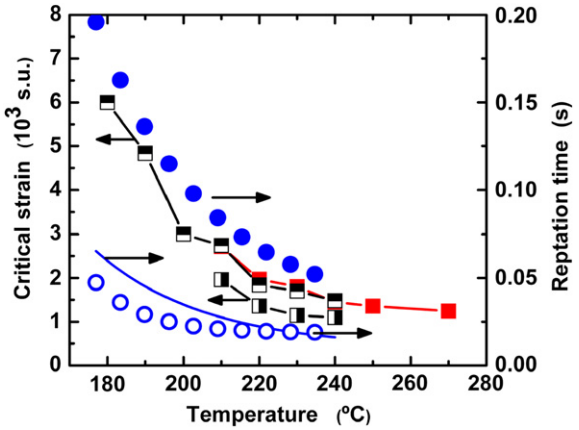

Fig. 3. Temperature variation of critical strain and reptation time. Filled squares - strain needed to saturate crystallization evaluated from experiments in the shear DTA; horizontal and vertical half-filled squares are the strain at the onset of steady state evaluated in the rheometer with parallel-plate and cone-and-plate configurations, respectively. Filled circles - reptation time of relaxed melts with the melt memory erased; open circles - reptation time of melts sheared up to steady state with a shear rate of 30 s^{-1}. The solid line is the division by three of reptation time for relaxed melts. Experimental errors of all these measurements are indicated in ref. [5].

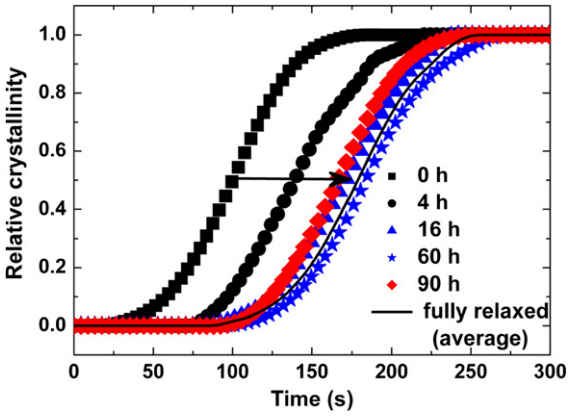

Fig. 4. Slowing down of quiescent iPP isothermal crystallization at 125 °C recorded with a shear DTA. Melt temperature: 220 °C. Cooling rate to crystallization temperature: −30 °C/min. Filled squares correspond to the quiescent crystallization of a pre-sheared melt at 220 °C with $\dot{\gamma}_w = 8.3\ s^{-1}$ and shearing time of 1200 s (average strain ≈ 9960 s.u., which is above the critical strain ≈ 1914 s.u.). Other symbols correspond to similarly pre-sheared melts, but with non-zero annealing times at the melt temperature. The sample is degraded after 90 h of annealing at 220 °C. Solid line represents the average crystallization curve obtained from a set of similar crystallization experiments for a fully relaxed melt (average half-crystallization time equal to 178 ± 5 s).

mobility. In principle, any one of these two effects, or a combination of both, could explain the slowing down of crystallization kinetics demonstrated in Fig. 4.

Results of Fig. 5 exclude the first possibility. Due to the physical impossibility of extracting samples for morphological analysis in the shear DTA, the same flow deformation history was imposed to samples prepared in a parallel plate rheometer (Physica MCR 300 (Paar Physica). Sample A (Fig. 5a) was heated up to 220 °C, the melt was allowed to relaxed, and the sample was cooled with a controlled cooling rate of 10 °C/min to room temperature. Sample B (Fig. 5b) was heated at the same temperature and sheared with a shear rate of 10 s^{-1} during 200 s, after which it was cooled, with the same cooling rate, also to the room temperature. Besides the existence of more β spherulites in Fig. 5b, no significant changes in the morphology are observed in these two figures. The fact that results of these Fig. 5a and b refer to samples cooled with a constant rate, while results of Figs. 2 and 4 refer to isothermal crystallization experiments, does not change the validity of the above conclusion. It was demonstrated that regardless the crystallization temperature [6,10], or the cooling rate used [11], saturation of crystallization from pre-sheared melts occurs always after deformation with the same strain.

Since, as demonstrated by the results of Fig. 5, annealing the melts does change significantly the nucleation density, we are left with the option of reduced chain mobility to explain the sluggish crystallization kinetics of relaxed melts. The validity of this conclusion is demonstrated below.

4. Discussion

We discuss first the validity of results described above and analyse possible error sources. Based on the experimental results presented, we discuss possible factors affecting the morphology of sheared polymers melts at steady state that could be responsible for the acceleration of crystallization kinetics described in Fig. 2. This discussion is complemented with a quantitative analysis of the factors affecting the different half-crystallization-time for the slowest and fastest crystallization kinetics results in Figs. 2 and 4. We conclude the discussion with a brief analysis and application of a model developed by Rubinstein and Obukhov that attempts to explain the memory effects in entangled polymer melts.

4.1. Validity of experimental results

The temperature variation of the strain required to saturate the crystallization, decreasing by increasing the sheared melt temperature (Fig. 3), suggests that a well-defined melt state should be responsible for that saturation. This melt state was identified with shear stress growth experiments as the steady state [5]. As indicated in Fig. 3 by horizontal half-filled squares, the temperature variation of the strain at the onset of steady state, evaluated with a parallel plate rheometer, has similar value and the same temperature variation as the strain that saturates crystallization. Results obtained with cone-and-plate configuration (vertically half-filled squares) are around 2/3 the values obtained with parallel plate configuration. The reason of this last result is that the average shear rate in a rheometer with parallel plate configuration is 2/3 the shear rate value at the edge of the plate. The agreement between the results obtained with these two configurations excludes slippage of polymer between plates as a possible source of error, and guarantees a laminar flow at steady state. Also, the suggested possible bonding of polymer chains to metal surfaces of capillary channel or to the rheometer plates, playing the role of grafted chains [12], acting as a lubricant and promoting chain slippage is excluded based on the above results obtained with the parallel plate and cone-and-plate configurations.

The results of Fig. 2 (or Fig. 4) cannot be assigned to the presence of impurities, nucleating agents or additives present in the commercial polymer sample used, such as those described, for example, by Byelov, Panine and de Jeu [13]. The same melt and crystallization temperature were used in these experiments. The only variable was the strain applied to the melt at 220 °C in the results of Fig. 2, and the annealing time of the melt at 220 °C in the results of Fig. 4. The concentration of nucleating agents and the exposure of their surfaces to the melt are the same in all experiments.

An additional possible artefact, namely the breaking of the nucleating agents present in polymer, by the effect of pressure exerted during flow, exposing new fresh surfaces that may act as nucleating agents promoting the acceleration of crystallization

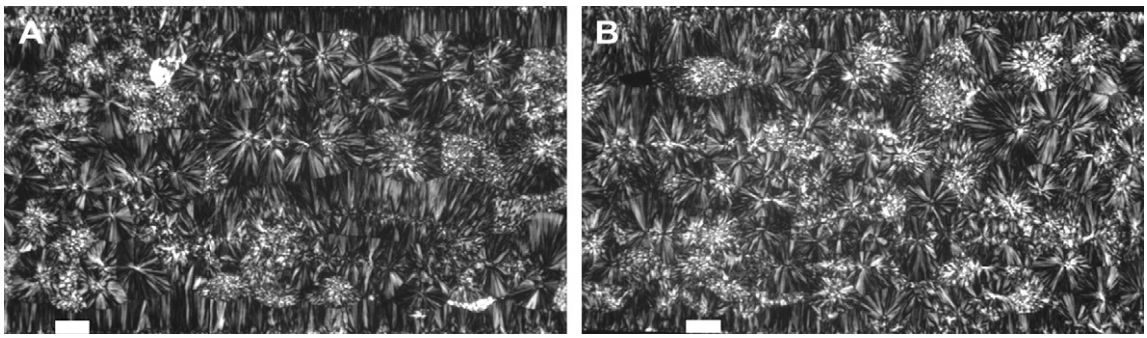

Fig. 5. Non-isothermal crystallization at −10 °C/min of molten iPP samples at 220 °C. (**A**) Relaxed melt. (B) Melt sheared up to the steady state with the shear rate of 10 s^{-1} during 200 s. After shearing the sample was cooled to room temperature.

kinetics observed in Fig. 2 is also excluded. If this was the case, the same fresh surfaces exist in the experiments described in Fig. 4 where a slowing down of crystallization kinetics is observed. One could then envisage a process by which the fragmented nucleating agents, separated from each other by the rotational component of shear flow, stick again. We do not consider likelihood this event.

Still another possible source of error is the pressure drop along the whole system. From iPP rheological data at 220 °C (power law exponent $n = 0.792$ and $K = 1063$) its value is 10 MPa, and the apparent shear stress at the capillary channel's wall is around 0.08 MPa. The ratio between isothermal compressibility and thermal expansion coefficient of iPP at 190 °C is $dT/dp = 1.504 \times 10^{-7}$ °C/Pa [14], which yields an increase in the melting temperature resulting from the pressure driven flow of around 1.5 °C, low enough for affecting the results here presented.

Therefore, results of Figs. 2 and 4 force us to consider the existence of two well-defined melt states, one responsible for the slowest crystallization kinetics and the other responsible for the fastest crystallization kinetics. We conclude that the former is a fully relaxed melt and the latter is a disentangled melt that resulted from the shearing up to the steady state.

4.2. Possible factors affecting the morphology of polymer melts at the two melt states

Understanding the relative difference of crystallization kinetics from the two melt states, and also the origin of melt memory effect, requires a precise understanding of polymer melt morphology and its variation with flow. One specific aspect that needs clarification is the unfounded assumption that polymer chains are stretched by shear flow, and that the orientation of polymer molecules with the flow direction promotes their alignment and chain interactions, increasing the number of stable nuclei and accelerating the crystallization kinetics [4]. It is known from experiments that the number of chain conformations aligned with flow direction increases by increasing the shear rate [15], but this increase does not affect the overall chain's shape [16,17]. Also, as shown below, in the timescale of our experiments, any segment orientation within the Rouse sequences relaxes almost instantaneously.

Experimental results demonstrate that the deformation of polymer chains in melts by shear flow is small. The chain's radius of gyration variation by shear, with respect to its value in a relaxed melt, increases up to maximum of 1.5, and at steady state it stabilizes at around 1.15 for a mixture of deuterated and hydrogenated PS [16]. The measured coil expansion ratio of 1,4 polybutadiene is much lower, around 1.02 [17]. Since the above measurements were obtained with deuterated chains of similar molecular weight to the polymer, it appears that the variation in the radius of gyration of a Gaussian chain segment between entanglements cannot exceed also the above experimental values. The assumption of chain stretch by shear flow at steady state seems therefore unfounded, without support from experimental results.

Further, as shown in Fig. 3, the longest relaxation time for this iPP sample at 220 °C is around 10^{-2} s. Any orientation induced to the chains by flow applied at the melt temperature relaxes within the Rouse relaxation time of the chain, around 2.26×10^{-5} s. This value is obtained after the following reasoning. The chain diffusion coefficient is $k_B T/\zeta_{chain}$, with $\zeta_{chain} = N_k\ \zeta_k$, where ζ_k is the Kuhn monomer friction coefficient, equal to 1.04×10^{-12} kg/s for iPP (estimated at $T = 460$ K). A chain of this iPP contains around 833 Kuhn monomers and D_{chain} is then 8.66×10^{-12} m^2/s. The iPP Kuhn monomer length is 11 Å, the Rouse relaxation time of the chain is approximately $\tau_R = \langle [r(t) - r(0)]^2 \rangle / 6D_{chain} \approx 2.26 \times 10^{-5} s$.

Results of Fig. 4 indicate that the effects imposed by flow to the polymer melt needs around 16 h to relax fully. On the other hand, because closing the entrance and exit valves takes around 5 s, and ~3 min more are need to cool the melt in the channel to the crystallization temperature (cooling rate of 30 °C/min), the acceleration of crystallization shown in Fig. 2 cannot be assigned also to any pre-orientation of chains in the melt. Chain relaxation is almost instantaneous in the timescale of our experiments reported in Figs. 2 and 4.

An additional discussion on the origin of melt memory requires knowledge of melt morphology at the two melt states. The longest relaxation time (or reptation time), evaluated from the crossing point between $G'(\omega)$ and $G''(\omega)$, of fully relaxed melts is longer than that of melts sheared up to steady state [5] – filled and open circles in Fig. 3, respectively. Because reptation time is related to the number of entanglements in the chain, $\tau_{rep} \approx \tau_R Z$, where τ_R is the Rouse relaxation time of the chain and Z the number of entanglements, this result indicates that for iPP around 2/3 of entanglements were destroyed during the transition to the steady state. The solid line in Fig. 3 is the division by three of reptation time values obtained for relaxed polymer melts, and it coincides with results obtained for melts sheared up to steady state.

Since these melts have only 1/3 of the entanglements existing in a fully relaxed, they have also lower viscosity. Fig. 6 demonstrates the different zero-shear rate viscosity in these two different melt states. These results were obtained in a rheometer with parallel plate configuration at 220 °C. Filled squares show the viscosity variation with shear rate of an initially relaxed melt. The zero-shear rate viscosity is around 1600 Pa.s. Open squares indicate the results obtained for pre-sheared melts up to the steady state with a constant shear rate of 30 s^{-1} during 100 s to guarantee the attainment of steady state. After this experiment, the melt, at the same temperature, was tested again with decreasing shear rates. The zero-shear rate viscosity of this melt is around 670 Pa.s and the physical reason for its lower viscosity, as demonstrated in Fig. 3, is the lower number of entanglements in melts sheared up to the

steady state. A similar result was obtained by Rastogi et al. for the viscosity of nascent polymer powders (disentangled) and commercial polymer grades (entangled) with similar molecular weight [18]. Upon heating, the distribution of entanglements is heterogeneous in the nascent powders and homogeneous in the commercial grades. We demonstrate below that this difference of viscosity between melt states with different degree of entanglement explains in part the acceleration in crystallization observed for sheared melts.

Results of Fig. 3 indicate similar temperature dependence for the critical strain and reptation time. They suggest a direct proportionality relationship between the critical strain and reptation time and that the proportionality constant, which should depend on the polymer chemical structure and chain architecture, is independent of temperature.

4.3. Possible factors affecting the acceleration of crystallization kinetics

In the Avrami's formalism, the half-crystallization time may be expressed as a function of the average nucleation density $\overline{N}$ and spherulite growth rate G as

$$\left(\frac{1}{t_{50\%}}\right) = \ln(2)^{-1/3}\cdot\frac{4\pi}{3}\frac{\rho_s}{\rho_l}\cdot(\overline{N})^{1/3}\cdot G_r = \alpha\cdot(\overline{N})^{1/3}\cdot G \qquad (1)$$

where ρ_s and ρ_l are the solid and liquid phase densities, respectively, and $\alpha = \ln(2)^{-1/3}\cdot(4\pi\rho_s/3\rho_l)$. In principle, we may have different nucleation density and spherulite growth rate for relaxed melts and melts sheared up to the steady state.

The ratio of the reciprocal half-crystallization time for samples crystallized from the two melt states is

$$\frac{(t_{50\%})_s}{(t_{50\%})_r} = \frac{(\overline{N}_r)^{1/3}\cdot G_r}{(\overline{N}_s)^{1/3}\cdot G_s} = \frac{(\overline{N}_r)^{1/3}\cdot\exp(-\Delta G_{d,r}/RT)\cdot\exp(-k_g/T\cdot\Delta T_r\cdot f)}{(\overline{N}_s)^{1/3}\cdot\exp(-\Delta G_{d,s}/RT)\cdot\exp(-k_g/T\cdot\Delta T_s\cdot f)} \qquad (2)$$

where the subscript r is for relaxed and s for sheared. We have considered in Eq. (1) and Eq. (2) an instantaneous nucleation of spheres and the spherulite growth rate expressed by the Laurizten and Hoffmann general equation, with ΔG_d representing the activation energy for transport of chain stems to the spherulite growth front, ΔT the supercooling degree, f the factor accounting for the variation of the enthalpy of fusion with temperature, and $k_g \propto \sigma\cdot\sigma_e/\Delta h_f^0$; σ and σ_e are the lateral and fold surface-energy, respectively, and Δh_f^0 is the enthalpy of fusion of the perfect crystal.

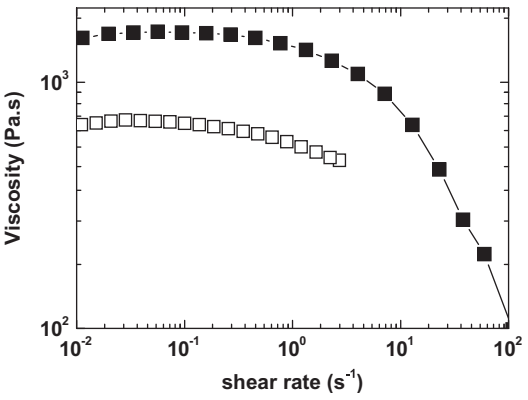

Fig. 6. Controlled shear rate scan from high to low shear rates performed in a parallel plate rheometer at 220 °C. Filled squares: relaxed melt. Open squares: melts pre-sheared with constant shear rate of 30 s^{-1} during 100 s to guarantee the attainment of steady state. After this experiment, the melt was tested again with decreasing shear rates.

Equation (2) allows us identifying three factors that may contribute to the different half-crystallization time of the samples crystallized at the same temperature from the two melts states: a different nucleation density, a variation in the supercooling degree by the effect of pressure imposed during flow, and different energy barriers for the transport of chain stems to the spherulite growth front. Before proceeding on with the separate analysis of each factor to find out the most relevant contribution for the different half-crystallization time, we make a brief analysis of literature results of crystallization from disentangled melts.

4.3.1. Crystallization from disentangled melts

The first step that should be followed to study the crystallization from disentangled melts is to quantify the number of entanglements existing in these melts. By definition, it is assumed that this number is zero, although it may change during heating. Our experimental results demonstrate that a iPP melt sheared up to the steady state has 1/3 the number of initial entanglements.

The kinetic process of the reconstruction of the entanglement network from a disentangled melt is unknown. Eventually, this knowledge will only be accomplished with a physical definition of entanglement. According to the experimental results of Rastogi et al. [18], the heating rate of the melt affects the entanglement process of a disentangled polymer. It is faster for higher heating rates. It was shown by us [5,10] – see also Figs. 2–4 –, and confirmed later by Lippits et al. [19], that disentangled melts crystallize faster than entangled melts. At the same crystallization temperature, the ratio between the half-crystallization time of relaxed melts and melts sheared up to the steady state evaluated from results of Figs. 2 and 4 is around 2. A difference of one order of magnitude was evaluated by Lippits et al. for the onset of the build up of storage modulus in heterogeneous (disentangled) melts, which occurs earlier, and in homogeneous (entangled) melts. We assign this difference of results to the different number of entanglements in our samples and in those of Lippits et al., which used nascent polymer powders.

Recent molecular dynamics simulations attempted to explain the development of entanglements in fully disentangled polymer melts [20]. Disentangled chains have an initial globular shape and, upon heating, acquire the random-walk-like conformation. It was found that, for short chains, the elastic network of entanglements is easily restored in a time faster than the time need for the chains to acquire their equilibrium conformation.

Due to the difficulty in obtaining disentangled melts with a well-defined number of entanglements, most studies about the effect of the number of entanglements on crystallization used pressure to produce extended chain crystals. Crystallization studies were then performed with these samples and compared with reference (entangled) samples previously submitted to the same thermal history cycle. Psarski et al. [21] found that spherulites in melts with lower number of entanglements growth faster (around 25–40%) but the nucleation density is reduced in comparison with fully entangled melts. The complete entanglement restoration requires, according to results of this work, between 25 and 30 min [21], proceeding much slowly than the molecular dynamics simulations results of short chains mentioned above [20]. Desorption of chains from the heterogeneities surfaces during the high pressure crystallization was considered as the factor behind the observed decrease of nucleation density.

Results of Yamakasi et al. [22–24], obtained with fractionated polyethylene samples and with nascent polymer powders, also crystallized under pressure, indicate a higher nucleation density for

disentangled melts. An empirical equation was presented to describe the nucleation rate variation with the number density of entanglements,

$$I(\nu_e) \propto \exp(-\gamma \nu_e) \tag{3}$$

where ν_e is the number density en entanglements, equal to one for a fully entangled sample, and γ is constant equal to 0.17 for PE [24]. We apply this equation below to our results.

4.3.2. Different nucleation density in the crystallization from relaxed and sheared melts

From data of Fig. 2 (or Fig. 4) the half-crystallization time for samples crystallized from relaxed melts and melts sheared up to the steady state is $t_r = 180$ s and $t_s = 101$ s. Considering now that the different nucleation density is the only relevant factor, we have

$$\overline{N}_s = \left[(t_{50\%})_s/(t_{50\%})_r\right]^3 \cdot \overline{N}_r = 5.8\overline{N}_r \tag{4}$$

This result means that nucleation density in samples crystallized from sheared melts should be 5.8 times that of samples crystallized from relaxed melts, and that the average spherulite radius of the former should around half ($r_s \cong 0.56 \cdot r_r$) that obtained in the crystallization from relaxed melts. Results of Fig. 5 demonstrate that this does not occur; the spherulite size is similar for samples crystallized from the two different melt states, which suggest similar nucleation rates.

We may further check this assessment with the application of the empirical equation of Yamakasi et al. [22–24], Eq. (3). Assuming the same γ constant for iPP (0.17), we evaluate the ratio of the nucleation rate between sheared and relaxed melts, knowing that $\nu_e = 1$ for relaxed melts and $\nu_e = 1/3$ for melts sheared up to the steady state. The result obtained is $I_s = 1.12 \cdot I_r$, confirming the results of Fig. 5 for the similar nucleation density and spherulite size in the crystallizations from the two melt states.

4.3.3. Different supercooling degree in the crystallization from relaxed and sheared melts

If the different supercooling degree is considered now as the factor responsible for this behaviour, we have

$$\Delta T_s^{-1} \cong \Delta T_r^{-1} + Tk_g^{-1} \cdot \ln\left[(t_{50\%})_s/(t_{50\%})_r\right] \tag{5}$$

For the crystallization temperature of 125 °C, and with $kg = 3.659 \times 10^5\ \mathrm{K}^2$ [25], the difference of supercooling degree between the crystallization from sheared and relaxed melts is $\Delta T_s - \Delta T_r = 4.4$K, which means that the observed decrease in the half-crystallization time in Fig. 2 could be explained if the pressure applied to the molten polymer during shear flow increases its melting temperature by 4.4 K. We have shown above that this increase is only 1.5 K. Although this factor may have some contribution for the acceleration of crystallization kinetics in sheared melts, it does not explain the results obtained.

4.3.4. Different activation energy for chain diffusion in the crystallization from relaxed and sheared melts

The additional remaining factor to consider is the decrease of activation energy for transport of chain stems to the growth front, which is

$$\Delta G_{d,s} - \Delta G_{d,r} = RT\ln\left[(t_{50\%})_s/(t_{50\%})_r\right] = -2.3 \times 10^3 J \cdot mol^{-1} \tag{6}$$

We show in Fig. 6 that melts sheared up to the steady state have lower viscosity than relaxed melts. In this case, the ratio of viscosity between sheared and relaxed melts is around 0.43.

We may assume then that the difference of viscosity between sheared and relaxed melts is the main factor behind the acceleration of crystallization shown in Fig. 2. The ratio of the two viscosities may be expressed as a function of the difference in the activation energy for transport of chain stems as $\eta_s/\eta_r = \exp[(\Delta G_{d,s} - \Delta G_{d,r})/RT]$, which yields a value of 0.57 (for $T = 220$ °C). This value is similar to 0.43 evaluated from the data of Fig. 6, and it indicates that the different rate of diffusion of chain stems in relaxed and sheared melts is the main factor behind the different crystallization rate from the two melt states. We must add to this contribution other minor effects for the small increase in the supercooling degree and slightly higher nucleation rate.

An apparently contradictory result to this conclusion was recently published by Maus et al. [26]. To understand the origin of precursor structures, and the melt memory effect, they performed NMR experiments on syndiotactic polypropylene. All NMR results indicate similar melt structures for melts with and without memory: static ^{1}H and ^{13}C spectra are similar; also the area of peaks associated to *tggt* and *gttg* sequences is similar for both melt types. This result was considered by the authors as the first experimental proof for the existence of "dormant" nuclei [27] that are sporadically activated on the same timescale as the crystallite growth. In agreement with previous results they found that samples with memory crystallize 15 K above the samples without memory, implying therefore higher nucleation and/or spherulite growth rate [26].

We cannot explain yet the reason of the apparent contradiction between the results of Maus et al. [25] and the results we have presented here and in other works [5,10]. Standard spin-echo experiments probing kilohertz motions through spin–spin (T_2) relaxation of the protons revealed differences between homogeneous (fully entangled) and heterogeneous melts [18]. It was found that the T_2 relaxation is independent of the heating rate in fully entangled melts while the disentangled melt relaxes faster when heated with a high heating rate, and slowly for heating with low heating rate. In principle, similar observation of the *T2* relaxation in a melt with memory should yield similar results to those of Rastogi et al. [18].

4.4. Results of a model for the melt memory in entangled polymers

Rubinstein and Obukhov proposed and formulated a model for explaining the origin of melt memory effect in entangled polymer melts [28]. Their reasoning was based on a model elaborated by Deutsch [29] that considered the effect of excluded volume interactions between diffusing chains in polymer melts, which allowed him, using ideas of reptation and tube model, to explain the 3.4 dependence of viscosity on the chain molecular weight (an alternative explanation by Doi [30] considered the contour length fluctuation of chain ends as the factor responsible for that variation). Implicit to this model, although not explicitly stated by his author, is the non-ideality of polymer chains in the molten state, which has been considered also recently by other authors [31,32].

In the model of Rubinstein and Obukhov it was considered that the origin of melt memory effect is in the excluded volume interactions between the chains in the melt. They argued that a reptating chain leaves a trace in the melt which manifests in the form of elastic distortions of the entanglement network. Relaxation of this elastic energy is made by the neighboring chains that are attracted to that trace reproducing the configuration of the first polymer chain. The development of this reasoning allowed to relate the melt relaxation time with the diffusion time, defined as the time need by a chain to diffuse a distance of the order of its radius of gyration. The relationship obtained was $\tau_{\mathrm{relax}} \sim \tau_{\mathrm{dif}} N^{1/3}$. According to this model, after the time τ_{relax} the elastic energy is fully relaxed.

We apply now this model to our experimental results. At 200 °C the reptation time for melts sheared up to the steady state is around

0.03 s. If we assume that relaxation is controlled by the longest chains in the melt, each chain with M_z molecular weight of this iPP has around 2711 Kuhn monomers, and its relaxation time is $\tau_{relax} \sim 14\tau_{dif}$. This time is far below the relaxation time need for erasing the melt memory effect in Fig. 4. The apparent reason for the failure of this model may be anticipated.

Although the philosophy behind the model sounds appealing, it evaluates the increase of melt elastic energy by the movement of a chain confined to a tube that is followed by the relaxation of surrounding chains, and the uncompensated elastic energy is $\approx k_B T$. It explains in principle the relaxation of elastic energy in an entanglement network with constant number of entanglements. Our results demonstrate that the network of entanglements in relaxed melts is different from that existing at steady state, where only 1/3 of the initial entanglements persist and a wider tube confines the chains' motion. It can be easily demonstrated, based on the results of Fig. 3, that the volume of a tube confining the chain's motion in a melt sheared up to the steady state is $\sqrt{3}$ the volume of a tube confining the same chain in a relaxed melt. Also, for explaining the long time need to erase the melt memory effect, we may anticipate that the uncompensated elastic energy must be higher than the thermal energy of the melt. We will discuss further this issue in future works.

We have not explained here the effect on precursor structures of shear flow, neither provided a physical definition of these structures. As mentioned in a previous work [5], it is our understanding that first, we have to have a clear definition of the polymer melt morphology and discuss clearly and openly the question of ideality in polymer melts. We think that this discussion may contribute to define physically what entanglements are and, still according to our view, contribute to a better understanding of precursor structures. After all, we have to consider how structures with some degree of order (the precursors) coexist in dynamic melt with entanglements, and reach their maximum efficiency in melts sheared up to steady state.

As stated by de Gennes, "some strange things happen in polymer melts for times longer than the terminal time (reptation time). Memory effects are present for many hours, in samples where the terminal time is smaller than 1 min" [33]. He presented a conjectural explanation for long time memory effects in melts, and considered that the origin of this behaviour results from tight knots that are reeled in from both ends. Here conjectured still, without support of any physical argument, that these tight knots are very stable and persist for long time after heating the sample above its melting temperature. If this were the case, then the interaction energy involving a tight knot would be much higher than the melt thermal energy. It was demonstrated that the interaction energy between a chain and a loop, which may be considered an appropriate representation of tight knot, is below the thermal energy of the melt [34], which means also that representation of entanglement effects with chain loops cannot explain elasticity in polymer melts. Other explanations have therefore to be found for clarifying the molecular origin of melt memory. As stated in the previous paragraph, according to our understanding, they require discussing the ideality of polymer melts and the physical nature of entanglements.

5. Conclusion

Two opposite effects are described in this work. One is the acceleration in the crystallization kinetics of a melt pre-sheared above its melting temperature when the crystallization is recorded in quiescent conditions. Because the effect recorded results from the ability of the melt to store the memory of previous deformations, and because similar deformations are required to saturate the crystallization kinetics and establish a steady state in shear flow, having the same temperature variation, we conclude that the observed acceleration results only from the lower melt viscosity, and hence the higher chain mobility at steady state.

The other effect reported is the erasing of melt memory. Long annealing times at high melt temperatures are required for the melt relaxation and slowing down of crystallization kinetics. Again, because the same melt and crystallization temperatures are used in the opposite effect, we conclude that the slowing down of crystallization results from the melt viscosity increase.

A full explanation of these two opposite effects requires a detailed knowledge of polymer melt morphology. Results of the different relaxation times in the two melt states, the fully relaxed melt, where crystallization is slowest, and the sheared melt, where crystallization is fastest, indicate that the number of entanglements in the last is lower, this being the reason of the lower melt viscosity and fastest crystallization kinetics.

It is also demonstrated that the melt memory effect, usually reported in quiescent isothermal crystallization experiments by the slowing down in the crystallization kinetics with the increase of residence time at the melt temperature, results from the ability of polymer melts, when sheared above their melting temperature, to store the effects of previous deformations. This ability is limited when polymer melts reach the steady state. At this state, polymer chain segments cannot be oriented any more with the flow direction. This effect is manifested in the experiments here reported by the saturation of crystallization and also by other experimental results for the variation of the chain's radius of gyration with shear flow. By annealing the melts sheared up to a steady state, chain orientation gradually relaxes. The time needed to reach a fully relaxed melt state is surprisingly very large. Crystallization kinetics from fully relaxed melts is slowest.

Acknowledgments

We acknowledge Jean-Pierre Ibar for discussions, and the Portuguese Foundation of Science and Technology for funding the projects FCOMP-01-0124-FEDER-007151 (PTDC/CTM/68614/2006). Work supported by the European Community fund FEDER and project 3599/PPCDT.

Appendix

The shear DTA instrument contains three different sections, an accumulator, a conical coupling (and thermally insulating) valve and a capillary channel, see Fig. 7 [6]. The radius of the accumulator and capillary channels are 12.5×10^{-3} m and 1×10^{-3} m, respectively. The conical coupling valve has an upper radius of 12.5×10^{-3} m, lower radius of 1×10^{-3} m and the length is 20×10^{-3} m. At the start of the experiment all different sections are at the same temperature, which is set above the polymer melting temperature.

We explain first how controlled deformations are applied to the melt. The polymer at the accumulator is sheared with a pre-set apparent shear rate during a shearing time. The apparent shear rate at the accumulator wall is

$$\left(\dot{\gamma}_{w,\mathrm{accum}}\right)_a = 4Q_{\mathrm{accum}}/\pi R^3_{\mathrm{accum}} \tag{A.1}$$

and the volume flow rate is

$$Q_{\mathrm{accum}} = \pi R^2_{\mathrm{accum}} \cdot \Delta L / t_{\mathrm{shear}} \tag{A.2}$$

where ΔL is the length span by the piston in the accumulator during the shearing time t_{shear}.

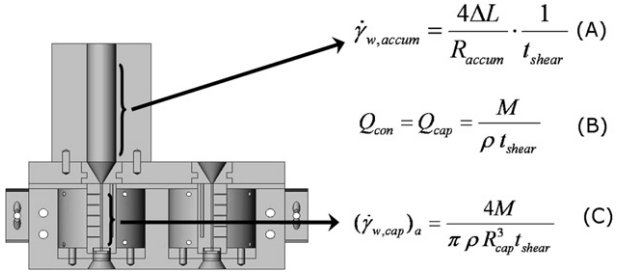

Fig. 7. Representation of the shear DTA instrument and the basic equation used to evaluate the total strain. The piston displacement ΔL is imposed by the program during the shearing time t_{shear}, and the shear rate at the accumulator wall is evaluated form Eq. (A). The weight (M) os the extruded sample during t_{shear} allows the evaluation of the shear rate at the capillary from Eq. (C), which allows also the evaluation of the shear rate in the conical valve from Eq. (B). These different shear rates are corrected with the Rabinowitsch correction. The melt residence time is each section is calculated, and from this the corresponding strain. The total strain is $\gamma = \gamma_{accum} + \gamma_{con} + \gamma_{cap}$.

The apparent shear rate in the capillary wall is

$$\left(\dot{\gamma}_{w,cap}\right)_a = 4Q_{cap}/\pi R_{cap}^3 \tag{A.3}$$

Assuming a conservative flow along the different sections of the shear DTA, $Q_{accum} = Q_{cap}$, the length that the piston in the accumulator should span to impose a programmed shear rate at the capillary wall during the shearing time is obtained from equations (A.2) and (A.3) as

$$\Delta L = \frac{R_{cap}^3}{4R_{accum}^2} \cdot \left(\dot{\gamma}_{w,cap}\right)_{a,program} t_{shear} \tag{A.4}$$

Typical shear rates used in the capillary channel are 5 s^{-1}. It is known from shear stress growth experiments performed with parallel plates in a rheometer that isotatic polypropylene at 220 °C, sheared at 5 s^{-1}, reaches a steady state after 400 s of shearing time [5], corresponding to a strain of 2000 s.u.

To impose a shear rate at the capillary channel wall of 5 s^{-1}, and considering a shearing time in the accumulator of 400 s, the piston would have to move a distance of 3.2 mm – equation (A.4). Since the polymer residence time in the capillary measurement point (30 mm after the entrance) is 24 s – Eq. (A.7) below –, it results that the strain in the capillary is only 120 s.u, far below the 2000 s.u. need to establish the steady state. Further, for the piston displacement in the accumulator of 3.2 mm during the shearing time of 400 s, the shear rate at the accumulator wall is only 2.56×10^{-3} s^{-1}. The addition of the strain values at the different sections of the shear DTA does not lead to any improvement. Therefore, in a conservative flow system, we could never be able to achieve the values of strain need to reach the steady state.

We analyzed also the non-conservative flow in the instrument, which results from two operative reasons that contribute to the escaping of material at the conical valve junction with the capillary channel. One is the need to have a worked loose for opening and closing the valve, and the other results from the thermally insulating block in which the conical valve is assembled. When this valve is closed, the capillary channel becomes thermally insulated from the accumulator allowing therefore cooling the capillary to a specific temperature, or with a controlled cooling rate (maximum 30 °C/min).

The shear rate the walls of the accumulator and capillary are evaluated independently. The former is done by a programmed control of piston displacement speed during the time t_{shear}, and the latter is done by weighting the material extruded during this time.

The way how the shear rates at the different sections of the instrument are evaluated and the evaluation of the total strain are indicated next. It must be stressed that the above evaluations did not considered the Rabinowitsch correction of the apparent shear rate values. This correction is considered also below.

The shear rate in the accumulator is precisely set by the program (Fig. 7), according to

$$\left(\dot{\gamma}_{w,accum}\right)_a = \frac{4\Delta L}{R_{accum}} \cdot \frac{1}{t_{shear}} \tag{A.5}$$

The accuracy of this setting is determined by step motor used in the control of the piston movement, which is better than 10^{-3} mm.

The shear rate at the capillary is evaluated by weighting the sample extruded during the shearing time, t_{shear},

$$\left(\dot{\gamma}_{w,cap}\right)_a = \frac{4Q_{cap}}{\pi R_{cap}^3} = \frac{4M}{\pi\rho R_{cap}^3 t_{shear}} \tag{A.6}$$

where ρ is the material density at the temperature at which extrusion took place. Since the volume flow rate is low and the shearing time is long, we consider that this shear rate is accurately evaluated.

One assumption only was made on the evaluation of the different shear rates, which was that the volume flow rate in the capillary is the same as in the conical valve,

$$Q_{con} = Q_{cap} = \frac{M}{\rho t_{shear}} \tag{A.7}$$

The residence time in the conical valve is then

$$t_{res,con} = \frac{\pi h\left(R_{accum}^2 + R_{cap}^2 + R_{accum}R_{cap}\right)}{3Q_{cap}} \tag{A.8}$$

where h is the length of the conical channel (20 mm). Typical values of this time are $\sim 10^{-1}$ s. The apparent shear rate at the conical valve wall was evaluated at its average radius (6.75 mm) from

$$\left(\dot{\gamma}_{w,con}\right)_a = \frac{4Q_{con}}{\pi\overline{R}_{con}^3} \times f_{geom} = \frac{4M}{\pi\rho\overline{R}_{con}^3 t_{shear}} \times f_{geom} \tag{A.9}$$

with the geometrical correction factor given by [35],

$$f_{geom} = \left[\frac{1 - \left(R_{cap}/R_{accum}\right)^3}{3\left(R_{accum}/R_{cap} - 1\right)}\right]^{3/4} \tag{A.10}$$

For evaluating the total strain we need to know the residence time in the capillary and accumulator. They are given by

$$t_{res,cap} = \frac{30 \times 10^{-3}\pi R_{cap}^2}{Q_{cap}} \tag{A.11}$$

and

$$t_{res,accum} = t_{shear} - \left(t_{res,cap} + t_{res,con}\right) \tag{A.12}$$

respectively, where the factor 30×10^{-3} refers to the measurement point of the thermocouple placed at the middle of the capillary channel.

Equations (A.5), (A.6) and (A.9) allow us to evaluate the apparent shear rate values at the different sections of the shear DTA. These values are corrected with the Rabinowitsh correction using values of the power law index obtained from flow curves recorded in a rheometer at the same temperature of the shear DTA. The strain at each section is evaluated considering the corresponding residence time, which is evaluated from equations (A.8), (A.11) and (A.12).

To illustrate the application of the above equations, consider one experiment described in Fig. 3 – shearing an iPP melt at 220 °C, $\rho = 743.9$ kgm^{-3} with a constant shearing time of $t_{shear} = 60$ s. We use equation (A.5), and set an apparent shear rate in accumulator's

wall of $(\dot{\gamma}_{w,\mathrm{accum}})_a = 5.13 \times 10^{-3}\ \mathrm{s}^{-1}$ to evaluate the required piston displacement. For this temperature and shear rate, the power law index is $n = 0.864$, the Rabinowitsh correction 1.039, the real shear rate at the wall of the accumulator is $\dot{\gamma}_{w,\mathrm{accum}} = 5.33 \times 10^{-3}\ \mathrm{s}^{-1}$, the residence time in the accumulator is $t_{\mathrm{res,accum}} = 38$ s, and the strain in the accumulator is $\gamma_{\mathrm{accum}} = 0.203$ s.u..

The evaluation of the strain value at the conical valve leads to a value of $\gamma_{\mathrm{con}} = 3.0$ s.u.. The measured weight of the sample extruded by the capillary channel during the shearing time of 60 s is $M = 1.95 \times 10^{-4}$ kg. The apparent shear rate in the capillary wall evaluated with equation (A.6) is $(\dot{\gamma}_{w,\mathrm{cap}})_a = 5.56\ \mathrm{s}^{-1}$. Using the same Rabinowitsh correction as above, we have for the real shear rate at the capillary wall $\dot{\gamma}_{w,\mathrm{cap}} = 5.78\ \mathrm{s}^{-1}$. The residence time at the capillary evaluated with equation (A.11), with Q_{cap} evaluated from experimental results with Eq. (A.7), is $t_{\mathrm{res,cap}} = 21.6$ s, and the strain at the capillary is $\gamma_{\mathrm{cap}} = 125$ s.u.. The overall strain is 129 s.u.. This strain value could be attained after a shearing time of 22 s. As the results of Fig. 2 and others shown in ref. [5] and [10] demonstrate, much higher shearing time is need to saturate crystallization recorded by a thermocouple, whose tip is at the capillary wall of the shear DTA, and to reach the steady state in the rheometer experiments. Since similar metal walls are used in the capillary channel of the shear DTA and in the plates of the rheometer, and their surfaces are not atomically smooth, our results suggest that melt morphology and flow behaviour may also be affected by surface roughness. This issue will be explored in future works. As shown in Fig. 3, the agreement between shear DTA and rheometer results is obtained when the strain at the capillary wall is multiplied by the overall shearing time. Similar procedure was applied to all curves indicated in Figs. 3 and 4, as well as in other results of other works [5,10,11].

References

[1] Alfonso GC, Ziabichi A. Colloid Polym Sci 1995;273:317–23.
[2] Häfele A, Heck B, Hipler T, Kawai T, Hohn P, Strobl G. Eur Phys J E 2005;16:217–24.
[3] Azzurri F, Alfonso GC. Macromolecules 2008;41:1377–83.
[4] Somani RH, Yang L, Hsiao BS. Physica A 2002;304:145–57.
[5] Martins JA, Zhang Wd, Brito AM. Macromolecules 2006;39:7626–34.
[6] Martins JA, Zhang Wd, Brito AM, Infante U, Romero M, Soares FO. Rev Sci Instrum 2005;76:105105.
[7] Liedauer S, Eder G, Janeschitz-Kriegl H, Jerschow P, Geymayer W, Ingolic E. Inter Polym Process 1993;8:236–44.
[8] Kumaraswamy G, Issaian AM, Kornfield JA. Macromolecules 1999;32:7537–47.
[9] Kimata S, Sakurai T, Nozue Y, Kashara T, Yamaguchi N, Karino T, et al. Science 2007;316:1014–7.
[10] Zhang W, Martins JA. Macromol Rapid Commun 2006;27:1067–72.
[11] Zhang W, Martins JA. Polymer 2007;48:6215–20.
[12] Brochard F, de Gennes PG. Langmuir 1992;8:3033–7.
[13] Byelov D, Panine P, de Jeu WH. Macromolecules 2007;40:288–9.
[14] Fernadéz M, Muñoz ME, Santamaría A, Syrjälä S, Aho J. Polym Test 2009;28:109–13.
[15] LeDuc P, Haber C, Bao G, Wirtz D. Nature 1999;399:564–6.
[16] Bent JF, Hutchings LR, Richards RW, Gough T, Spares R, Coates PD, et al. Science 2003;301:1691–5.
[17] Noirez L, Mendil-Jakani H, Baroni P. Macromol Rapid Commun 2009;30:1709–14.
[18] Rastogi S, Lippits DR, Peters GWM, Graf R, Yao Y, Spiess HW. Nat Mater 2005;4:635–41.
[19] Lippits DR, Rastogi S, Höhne GWH, Mezari B, Magusin PCMM. Macromolecules 2007;40:1004–10.
[20] Vettorel T, Kremer K. Macromol Theory Simul 2010;19:44–56.
[21] Psarski M, Piorkowska E, Galeski A. Macromolecules 2000;33:916–32.
[22] Yamakasi S, Hikosaka M, Gu F, Ghosh SK, Arakari M, Toda A. Polym J 2001;33:906–8.
[23] Yamakasi S, Hikosaka M, Toda A, Wataoka I, Gu F. Polymer 2002;43:6585–93.
[24] Yamakasi S, Gu F, Watanabe K, Okada K, Toda A, Hikosaka M. Polymer 2006;47:6422–8.
[25] Mark JE. Physical properties of polymers handbook. Am Inst Phys; 1996.
[26] Maus A, Hempel E, Thurn-Albrecht T, Saalwächter K. Eur Phys J E 2007;23:91–101.
[27] Janeschitz-Kriegl H, Ratajski E. Polymer 2005;46:3856–70.
[28] Rubinstein M, Obukhov SP. Phys Rev Lett 1993;71:1856–9.
[29] Deutsch JM. J Physique (Paris) 1987;48:141–50.
[30] Doi M. J Polym Sci Polym Phys Ed 1983;21:667–84.
[31] Wittmer JP, Beckrich P, Crevel F, Huang CC, Cavallo A, Kreer T, et al. Comput Phys Commun 2007;177:156–9.
[32] Dollase T, Graf R, Heuer A, Spiess HW. Macromolecules 2001;34:298–309.
[33] de Gennes P. Macromolecules 1984;17:703–4.
[34] Martins JA. Macromol Theory Simul 2010;19. doi:10:1002/mats.201000005.
[35] Michaeli W. Extrusion dies for plastics and rubbers: design and engineering computations. Munchen: Carl Hanser Verlag; 2003.